HHS Public Access

Author manuscript

Small. Author manuscript; available in PMC 2023 September 01.

Published in final edited form as:

Small. 2022 September ; 18(36): e2106896. doi:10.1002/smll.202106896.

Hydrolytically degradable microgels with tunable mechanical properties modulate the host immune response

María M. Coronel,
Woodruff School of Mechanical Engineering and Petit Institute for Bioengineering and Bioscience, Georgia Institute of Technology; Atlanta, GA, USA

Karen E. Martin,
Woodruff School of Mechanical Engineering and Petit Institute for Bioengineering and Bioscience, Georgia Institute of Technology; Atlanta, GA, USA

Michael D. Hunckler,
Woodruff School of Mechanical Engineering and Petit Institute for Bioengineering and Bioscience, Georgia Institute of Technology; Atlanta, GA, USA

Pranav Kalelkar,
Woodruff School of Mechanical Engineering and Petit Institute for Bioengineering and Bioscience, Georgia Institute of Technology; Atlanta, GA, USA

Rahul M. Shah,
Wallace H. Coulter Department of Biomedical Engineering, Georgia Institute of Technology; Atlanta, GA, USA

Andrés J. García
Woodruff School of Mechanical Engineering and Petit Institute for Bioengineering and Bioscience, Georgia Institute of Technology; Atlanta, GA, USA

Abstract

Hydrogel microparticles (microgels) have emerged as an attractive approach for therapeutic delivery because of their modularity, injectability, and enhanced integration with the host tissue. Multiple microgel fabrication strategies and chemistries have been implemented, yet manipulation of microgel degradability and its effect on *in vivo* tissue responses remain underexplored. Here, we report on a facile method to synthesize microgels crosslinked with ester-containing junctions that affords tunable hydrolytic rates. Monodisperse microgels of maleimide-functionalized poly(ethylene glycol) are generated using droplet microfluidics crosslinked with thiol-terminated, ester-containing molecules. Tunable mechanics are achievable based on the ratio of degradable to nondegradable crosslinkers in the continuous phase. Degradation in an aqueous medium leads to microgel deformation based on swelling and a decrease in elastic modulus. Furthermore, degradation byproducts are cytocompatible and do not cause monocytic cell activation under noninflammatory conditions. These injectable microgels possess a time-dependent degradation

andres.garcia@me.gatech.edu .

Supporting Information

Supporting Information is available from the Wiley Online Library or from the author.

on the order of weeks *in vivo*. Lastly, evaluation of tissue responses in a subcutaneous dorsal pocket shows a dynamic type-1 like immune response to the synthetic microgels, driven by IFN-γ expression, which can be moderated by tuning the degradation properties. Collectively, this study demonstrates the development of a hydrolytic microgel platform that can be adapted to desired host tissue immune responses.

Keywords

microgels; PEG-4MAL; degradation; microfluidics

1. Introduction

Hydrogel microparticles (microgels), either in suspension or as building blocks for granular bulk hydrogels, have emerged in recent years as an attractive platform in biomedical applications because of their highly tunable mechanical properties, injectability, and a high degree of tissue integration[1,2]. One of the design parameters that is directly coupled to microgel physical properties (e.g. stiffness, mesh size, etc.) is the degradation rate. Mechanisms for degradable crosslinking of polymers can be broadly categorized into enzymatic, photodegradable, hydrolytic, or a combination of these conferring varying degrees of control over degradation rates[3–8]. The majority of these methods are dependent on stimuli that are not easily controlled, spatially nor temporally[9].

The application of ester-containing linkers offers a degradation mechanism based on hydrolytic cleavage of the ester bond. Degradation can be controlled by polymer content, macromer molecular weight, crosslinking density, and hydrophobicity of the ester labile linker[9,10]. In contrast to hydrogels with enzymatic degradation, the hydrogels developed through this approach are degradable through hydrolysis, allowing for consistent degradation profiles dependent solely on the adjustable physical, mechanical, and chemical properties of the hydrogel[9]. Whereas bulk gels have previously been engineered with hydrolytically degradable crosslinkers[9,11–13], this modality has yet to be translated to microgels fabricated through microfluidic-based polymerization.

The ability to incorporate degradability into the hydrogel network constitutes a major advantage for regenerative medicine and immunoengineering applications, as material persistence and mechanical properties will regulate the tissue response to the implant. The immune response to a biomaterial will ultimately determine the fate of the implanted material, whether it is integrated into the local tissue or walled off by the foreign body response (FBR). Initially, following biomaterial implantation, an inflammatory type 1 injury response will develop near the material, driven by pro-inflammatory mediators IFNγ and TNFα. Pro-regenerative biomaterials then drive a transition to a type 2 immune response, promoting M2 ($CD206^+$) macrophage polarization and T helper 2 cells infiltration via IL-4 signaling [14]. On the other hand, the host response to synthetic implants is typically characterized by a foreign body reaction that primarily activates mononuclear phagocytes [15,16] and other cells involved in executing type 3 immune responses[17]. Activated macrophages and Th17 cells secrete TGFβ and other factors that recruit fibroblasts, promote

their differentiation to myofibroblasts, and drive fibrosis at the implant surface. Recently, more complex interactions between different immune populations of varying phenotypes have been implicated in response to biomaterials[18–20]. However, this characterization pertains mostly to bulk hydrogel implants with relatively little research on the effect of microgel implantation and degradation on local tissue responses.

Herein, we present a fabrication approach based on flow-focusing droplet generation that produces monodisperse hydrolytically degradable microgels with modular mechanical and degradation profiles dependent on the introduction of a labile ethylene linker, ethylene glycol bis(mercaptoacetate)(EGBMA). We demonstrate that controlled hydrogel degradation profiles can be achieved by tuning the ester concentration in the hydrogel microparticle via the addition of varying molar concentrations of EGBMA to a nondegradable linker in the continuous flow phase. The addition of EGBMA did not influence macrophage polarization *in vitro* while it promoted degradation *in vivo*. Additionally, we characterize the effects of degradability on tissue responses to the microgel suspension implant. We demonstrate that control over the degradation profile of the microgel suspension can modulate type 1 immune responses to the implant.

2. Results

2.1. Addition of ester-containing dithiol molecules generates hydrolytically degradable microgels

Hydrolytically degradable microparticles (i.e., microgels) were fabricated by droplet segmentation using a flow-focusing microfluidic device, as previously reported[21]. The PEG-4MAL macromer was functionalized with a linear PEG-FITC via Michael type addition for particle tracking, prior to segmentation in the microfluidic device. Pumping of the aqueous phase (containing the functionalized macromer) into the microfluidic device-generated droplets that were subsequently covalently crosslinked with a continuous phase of oil containing small dithiol molecules: dithiothreitol (DTT) and ethylene glycol bis(mercaptoacetate)(EGBMA). The addition of EGBMA allowed for the incorporation of a hydrolytically labile ester linker (Figure 1a). We varied the concentration of EGBMA in the continuous crosslinking phase from 0.25, 0.5 to 1.0 mM and held the concentration of DTT constant at 15 mM. ^{1}H molecular diffusion nuclear magnetic resonance (NMR) of the microgels revealed the absence of maleimide groups in the crosslinked PEG-4MAL macromer, indicating that the maleimide groups in the microgel droplet are efficiently reacted after on chip crosslinking (Figure S1).

Maintaining the flow rates constant for all conditions for a device with a 200 μm nozzle led to monodisperse microgel particles averaging 208 μm (CV 8%) in diameter when only implementing DTT in the crosslinking phase (Figure 1b). Addition of EGBMA to the crosslinking solution generated monodisperse microgel populations (Figure 1c–e, CV <10% for all groups), with microgels ranging in size from 219 to 270 μm diameter. EGBMA crosslinked microgels were 4, 10, and 33% larger in diameter at 4 hr post-fabrication than DTT only microgels, with significant swelling in the highest concentration EGBMA group when compared to the DTT control (Figure 1 f–g, $p<0.0001$ DTT vs 1.0 mM EGBMA). Macromer functionalization with PEG-FITC was equivalent across groups as

seen by mean fluorescent intensity measurements of the microgels post-fabrication (Figure 1 b–e, inset), indicating that differences in swelling can be attributed to the presence of the EGBMA linker and not the availability of the maleimide group for crosslinking. By day 30, DTT crosslinked microgels had reached an equilibrium size which was 6% higher than the initial microgel size, whereas EGBMA/DTT microgels with the medium and highest concentration of the labile crosslinker had swollen 26% and 46% greater than their initial sizes, respectively (Figure 1g, $p=0.01$ DTT vs 0.5 mM EGBMA, $p<0.001$ DTT vs 1.0 mM EGBMA). Microgel degradation was also assessed by tracking the amount of PEG-FITC released into solution, as the PEG-FITC is covalently linked to the PEG-4MAL macromer and can only be released from the hydrogel network by hydrolysis of EGBMA. PEG-FITC release results agree with swelling experiments, whereby the 1.0 mM EGBMA crosslinked microgels released PEG-FITC at a faster rate than the lower EGBMA concentrations, while the fully nondegradable control followed a small release of trapped PEG FITC, tailed by no PEG-FITC present in solution as expected.

Lastly, we determined the effect of EGBMA on the mechanical properties of the resulting microgels via pressure-induced deformation through a tapered microcapillary[22] (Figure S2). The microgel is deformed by a pressure differential across the microgel lodged at the end of the microcapillary. As the pressure differential increases, the microgel undergoes radial compressive strain and axial elongation (Figure 1i). The shear stress and strain can be determined using the taper angle, edge contact length, and average diameter when the microgel is at equilibrium (Figure 1j). Calculation of shear modulus, G, in this equilibrium state demonstrated no differences in elasticity of the microgels after 4 hr post-fabrication, with values ranging from 20–22 kPa for all groups tested. After 72 hr in solution, shear modulus decreased with increasing EGBMA concentration in the microgels, with a reduction in moduli from 20 kPa to 14 kPa (28% reduction) in the highest degradable linker group (Figure 1k, $p<0.0001$ vs DTT); by day 7, elastic modulus had decreased by 61% (8 kPa) in the highest degradable linker group, a behavior explained by reduced crosslink density due to hydrolysis of ester linker. Collectively, these data demonstrate no differences in effective crosslink density immediately following fabrication, while elastic properties of the microgels exhibit time-dependent decreases based on EGBMA hydrolysis and loss of network crosslinks. Furthermore, the results provide evidence of the consistency of the flow-focusing microfluidic platform in fabricating physically and mechanically homogenous microgels.

2.2. Microgel degradation and by-products do not induce monocyte activation *in vitro*

To assess the effects of hydrolytic degradation products of EGBMA/DTT-crosslinked hydrogels on cell viability and activation, the RAW 264.7 mouse macrophages cell line was grown in the presence of the different microgel formulations for over seven days. The presence of the microgels, and fabrication byproducts (e.g. any encapsulated DTT, or byproducts of hydrolysis) were not toxic to this cell line (Figure S3). These results are consistent with our previous work demonstrating no toxicity related to DTT crosslinking for encapsulated cells or cells co-culture with fully crosslinked microgels[21,23,24].

To assess the effects of microgels on immune cell polarization *in vitro*, we set up a co-culture system involving primary monocytes derived from the bone marrow of C57BL/6J mice with different formulations of crosslinked microgels. Polystyrene beads (PS) of similar size (200 μm) and at the same concentration per well were included as a negative control, as they have been shown to not induce cellular activation[25]. Furthermore, an IL-4-polarized M2 regulatory phenotype was included as a positive control, as exposure of macrophages to bulk PEG hydrogels has been shown to shift cell polarization towards a regulatory phenotype in the absence of adhesion cues and inflammatory signals[26]. Microparticle-containing groups exhibited similar cell viability following 48 hr of co-culture with all microgel formulations or PS (Figure 2a), while the addition of IL-4 led to an increase in cell numbers in the co-culture. No changes in the expression of CD45, F4/80, and regulatory marker CD206 were observed in the presence of PS or PEG-based microgels after two days of co-culture (Figure 2 b–d). In addition, the overall expression of these markers was equivalent after 4 days of co-culture (Figure S4 a–d). These findings indicate that changes in microgel elastic properties and size or degradation products do not induce any phenotypic changes in macrophage marker expression under noninflammatory conditions *in vitro*.

2.3. Subcutaneous microgel implantation leads to controlled degradation *in vivo*

To test the ability of EGBMA/DTT-crosslinked hydrogels to be degraded *in vivo*, microgels were fabricated as described above but the PEG-FITC tracker was replaced by a linear PEG of the same molecular weight containing a near-infrared dye for *in vivo* tracking. Microgels were injected into subcutaneous pockets in the dorsum of albino mice (to avoid attenuation of signal detection by melanin pigmentation[27]). The degradation of the microgels was tracked via *in vivo* fluorescent imaging (IVIS) (Figure 3a). Normalized radiant efficiency tracking over time demonstrates a decrease in fluorescence signal that is dependent on EGBMA concentration (Figure 3b). Notably, while there was a decrease in signal intensity in the DTT-crosslinked group, intensity values post-explant were comparable to day 1 values, demonstrating no degradation in this group as expected (Figure 3b, post-explant values after dashed lines, $p=0.44$). No differences in fluorescence signal among microgel formulations were observed on day 1 post-injection (Figure 3c), yet by day 9, fluorescence signal was significantly lower in microgel formulations containing the intermediate and highest concentrations of EGBMA crosslinker (Figure 3d, $p= 0.008$, $p= 0.0001$ vs DTT respectively). On day 25, signal intensity was 26%, 17%, and 12% of the original signal, a decrease directly proportional to the EGBMA linker concentration (Figure 3e, $p=0.0004$, $p<0.0001$, $p<0.0001$ vs DTT). Thus, IVIS imaging confirmed that microgels crosslinked with EGBMA degrade *in vivo*, and this degradation occurs over several weeks.

2.4. Degradation properties regulate immune response to microgels *in vivo*

We hypothesized that degradation and changes in the mechanical properties of the microgels due to swelling and hydrolysis of the ester-containing linker would influence immune responses to the implants. We injected all four different microgel formulations into subcutaneous dorsal pockets of BALB/cJ mice and retrieved the tissue on day 7 for multiparametric flow analysis. This time point was chosen as it had demonstrated differences in mechanical properties and degradation profiles among the materials being tested. Furthermore, to assess how degradability and dynamic changes in mechanical

properties influence the cellular environment, we focused our analysis on comparisons between non-degradable (DTT) and the three different degradable formulations. Myeloid cell populations (CD45+CD11b+) were dominant at the injection site in the microgels crosslinked with DTT compared to the degradable microgels containing 1.0 mM EGBMA (Figure 4a–b, p=0.018). Phenotyping of subpopulations within the myeloid compartment revealed differences in the presence of F4/80+ macrophages as a function of microgel crosslinker formulation (Figure 4c–d, p=0.008). Measuring activation of this cell population based on cell expression of major histocompatibility complex class II (MHCII) revealed no differences among microgel formulations (Figure 4e–f), yet intensity expression of this marker was greatest in the DTT crosslinked group when compared to the highest degradable microgel formulation (Figure 4f, p=0.03 DTT vs 1.0 mM EGBMA). Further analysis of macrophage polarization using the M1- and M2-associated markers, CD86 and CD206, indicated an increased presence of M2 polarized F4/80-expressing macrophages in the nondegradable DTT group compared to all other degradable formulations (Figure 4h), suggesting that tissue responses to nondegradable nonphagocytable microgels are dominated at this time point by an M2-like phenotype, and this polarization can be regulated by the material degradation profile.

We next examined the effect of microgel formulation on the recruitment of T cells to the injection site. DTT-crosslinked microgels recruited a higher number of CD3+ cells to the implant pocket compared to degradable microgels (Figure 5 a–b). This lymphocytic response was dominated by CD4 helper cells, which were elevated in the presence of nondegradable microgels (Figure 5 c–d). Expression of activation markers CD25 and PD-1 (Figure 5 e–h) was also influenced by microgel formulation, with increased upregulation in surface expression of these markers observed in the nondegradable group compared to the degradable microgels. Overall, the enhanced presence of CD4 cells combined with an increased M2-like cell phenotype in the DTT group, suggests an interplay between these two cell populations in the tissue response to nondegradable PEG-based microgels. Moreover, microgel degradation profiles, including changes in mechanical properties, can modulate the recruitment and phenotype of specialized cell subpopulations altering host tissue responses to the biomaterial implant.

2.5. Microgel-induced cytokine milieu is dynamic and dominated by IFN-γ expression

To better understand the interplay of the immune environment with the microgel degradation profile, we implemented a multiplexing technique to investigate the cytokine and chemokine (hereon referred to as cytokines) milieu regulating T cell recruitment and macrophage polarization post-microgel injection. Additionally, given the high level of correlation between cytokines, and the potential confounding factor of mice age on cytokine release (4-week difference between first and last time point analyzed), we implemented a modular cytokine analysis method, CytoMod, to provide some context between cytokine clustering and the observed cell phenotypes, as opposed to evaluating individual cytokines at distinct time points[28,29]. Principal component analysis (PCA) of grouped cytokines identified two directions in cytokine profile, with the bulk of the variation in cytokine levels dictated by cytokines IFN- γ and IL-2 in one direction and G-CSF in the orthogonal direction (Figure 6a, vector direction and color represent the contribution to the PCA). Cytokine similarity

across all subjects was defined by their Pearson correlation coefficient (Figure 6b), whereby unsupervised hierarchical clustering was used to identify five cytokine modules (Figure 6c). A statistically significant correlation was seen in module 1, composed of cytokines and chemokines involved in inflammation and Th polarization responses (IFN- γ, IL-2, IL-4, IL-17, IL-10, IL-6, MIG, RANTES, M-CSF, LIX). A cytokine-specific score was computed between cytokine levels and the mean cytokine matrix of all subjects, which determined IFN-γ as the driving cytokine consistent with the previous PCA analysis. Correlation plots within this module indicate a statistically significant positive correlation among most of the cytokines (IL-2, IL-10, IL-6, LIX, M-CSF) and IFN-γ. Thus, a condition with a high expression of IFN-γ was relatively likely to display a high concentration of these other cytokines (Figure 6d).

Direct comparison of raw cytokine values for all conditions at all time points evaluated indicated dynamic profiles, with EGBMA-containing formulations presenting lower mean cytokine levels for most cytokines evaluated (Figure 6e–f, Figure S5–6). Nondegradable microgels resulted in increased expression of GM-CSF and G-CSF early post-injection (Figure 6e, Figure S5). By day 7, expression of other chemokines involved in immune cell recruitment such as M-CSF and monokine induced by IFN-γ (MIG) was reduced in the group with the highest EGBMA degradable linker compared to the nondegradable control (Figure S5–6). Expression of type 1-associated cytokines TNF-α and the IFN-γ driver IL-2 was also reduced in tissues exposed to degradable microgels (Figure S5–6). Of note, expression of the crucial type 2 cytokine IL-4 was dependent on the microgel formulation, with higher levels of IL-4 observed at all time points for the nondegradable microgel compared to all degradable formulations (Figure 6f). Additionally, no differences in expression of angiogenic factor VEGF were observed among formulations at the time points investigated (Figure S5). These results, combined with the multiparametric flow analysis of cell phenotypes at the injection site, indicate that responses to PEG-based nondegradable microgels are driven by type 1 immunity with a degree of cross-regulation by type 2 driving cytokine IL-4. Importantly, this response can be modulated by the introduction of labile ester groups that hydrolytically degrade *in vivo*.

Tissue response to microgel injections in the dorsum of albino mice were generally mild, with cell infiltrates surrounding the implant periphery (Figure S7). Of note, none of the implants showed signs of encapsulation, or cyst formation. Cellular deposition around the surrounding microgel implant was apparent at the host implant boundary at 4 weeks post-implantation (Fig S8). Qualitative assessment of images revealed a higher cellular density around the implant periphery of implants containing nondegradable microgels (DTT), compared to all formulations of degradable microgels. Immunohistochemistry for pan macrophage marker CD68 demonstrated and increased presence of CD68 expression in the DTT and 0.25 and 0.5 mM EGBMA conditions compared to the condition containing the highest concentration of EGBMA (1.0 mM EGBMA). These results are consistent with our flow cytometry assessments for myeloid populations (Figure 4).

3. Discussion and Conclusion

Strategies conferring degradability to microgels have taken advantage of degradable chains in the polymer backbone or labile crosslinker units to enable cleavage either via hydrolysis, enzymatic reaction, or dissolution. Previously, we generated protease degradable microgels for the delivery of angiogenic factors[6]. While these microgels were formed implementing droplet microfluidics, it required the design of a custom microfluidic device, given the crosslinking peptides' limited solubility in the continuous phase. Here, we present a fabrication strategy that takes advantage of ester hydrolysis to regulate the degradation of crosslinked PEG-4MAL microgels. In contrast to our previous approach, this strategy could be implemented in the same microfluidic device we had previously designed for the fabrication of nondegradable microgels, as the labile crosslinker unit can be added to the oil crosslinking phase. Thus, this strategy enables tuning of the degradation properties of the microgel product simply by adjusting the crosslinking feed.

We monitored hydrogel degradation by evaluating changes in physical and mechanical properties, including swelling, release of a PEG-FITC tag, and elastic modulus. As expected, changes in these parameters were directly related to the EGBMA crosslinker content, and thus the number of hydrolyzable groups. Immediately post-fabrication, microgels synthesized with the highest concentration of labile ester junctions swelled to ~140% of the nondegradable microgel control's size; however, no appreciable differences in elastic modulus were observed at this point. This could be explained by the fact that, to completely release the PEG-4MAL macromer, multiple ester bonds must be cleaved. Indeed, measurable changes in elastic modulus were first observed following 72 hr in aqueous buffer, when sufficient crosslinks had been cleaved and PEG-4MAL macromer dissolution into the aqueous medium had occurred. Differences were more pronounced with time and directly proportional to EGBMA content, demonstrating the tunability of this approach. While not tested in this study, it is known that the hydrophobicity and presence of carbon units between an ester and a thiol can affect the rate of ester hydrolysis[10,11,30]. Thus, the implementation of linkers with hydrophobic molecular units between the ester and the thiol group or alterations to the polymer density may provide further control over the degradation of hydrogels synthesized by this approach without any appreciable impact on the fabrication technique.

Material degradability, while highly desirable for biomaterial platforms, can lead to unwanted toxicity and immune activation responses that hamper their applicability in the clinic. In this study, no noticeable effects on cell viability were observed in any of the microgel formulations tested, suggesting that the presence of microgels or their degradation byproducts do not result in toxicity-induced cell death at a dosage of up to approximately 3 microgels/μL. Additionally, the size of the microgels implemented in this study (>200 μm) should prevent them from being phagocytosed by macrophages[31]; however, degradation by-products and partial internalization could still lead to macrophage polarization. Although changes in mechanical cues have demonstrated an effect on M1-like macrophage activation[32,33], changes in surface chemistry have been shown to have a higher influence on M2-like polarization[34,35]. In this study, neither the presence of EGBMA crosslinking units nor changes in mechanical properties had an impact on M2-associated

CD206 marker expression *in vitro*. We postulate that most of the unreacted crosslinking molecules were removed from the microgel suspension through the centrifugation/washing steps. Furthermore, at the microgel to cell ratio implemented, the concentration of the linker molecules in solution, due to hydrolysis, did not influence this marker expression.

Despite several strategies reported for degradable PEG-based hydrogels, few studies have reported that *in vivo* degradation rates can be orders of magnitude different those *in vitro*[13,36–38]. Indeed, protease-cleavable formulations that have been shown to rapidly degrade in culture do not degrade post-implantation[36]. Likewise, differences in degradation rates have also been observed in hydrolytic degradation, whereby the gradual hydrolytic degradation rates *in vitro* did not match the rapid degradation observed *in vivo*[13]. Here, using microgels labeled with a near-infrared dye, we demonstrated that DTT/EGBMA-crosslinked microgels degrade *in vivo*, with degradation times that span several weeks. This is consistent with the degradation rates observed in the *in vitro* studies and to other ester-containing bulk PEG hydrogels[10]. In subsequent studies, it will be important to evaluate how the addition of biological factors (e.g., adhesion ligands, encapsulated cells, or therapeutics) alters the rate of ester hydrolysis in these microgels.

Finally, tissue responses as a function of degradability were assessed in a subcutaneous dorsal model. This site provides an easily accessible location that can hold substantial microgel transplant volumes. Moreover, it permits the use of the same animal as its own internal positive control, as multiple independent microgel suspensions can be injected into different quadrants of the dorsum. Multiparametric flow analysis demonstrated degradation-dependent immune responses, with the enhanced presence of myeloid and T cells, in particular CD4+ cells, in the nondegradable formulation, consistent with other studies showing T helper cells driving responses to synthetic material implants[17,39]. Further evaluation of the cytokine environment provided additional insights into the diversity and complexity of the immune responses. In contrast to reports of an IL-17-driven immune response to synthetic bulk implants[17], we found that injections of synthetic microgel suspensions led to a prominent expression of IFN- γ which remained elevated for up to 4 weeks. Remarkably, unsupervised clustering of cytokine correlations identified IFN-γ as the dominant response driving cytokine communications. IFN- γ is one of the canonical cytokines driving type 1 immune responses[40], and it is primarily produced by activated T cells and promotes M1 polarization by STAT1 phosphorylation[41]. Evaluation of the macrophage cellular response acutely post-implantation of the microgel suspension revealed phenotypic characteristics that resemble more an M2-like phenotype (i.e., CD206 expression). This phenotypic plasticity suggests a shift in the microenvironment milieu leading to repolarization of IFN-γ-activated macrophages. Future work should investigate if indeed this repolarization is due to the presence of other cytokines in the immune response (i.e. persistence of IL-4), given that M1 polarization can prime the transition into distinct M2 phenotypes in response to IL-4[42]. Additionally, these studies were performed in BALB/cJ mice which have shown to have a genetic predisposition towards M2 polarization. Thus, a microgel-induced M2 phenotype cannot be generalized until tested in other strains[39].

Although type 1 cytokines seemed to be the primary driver of local tissue responses, our study suggests a reciprocal IL-4-driven response that should be further investigated. No

observable changes in IL-4 secretion even after 30 days post-injection were evident in the nondegradable implant. Notably, modulation of this immune response was possible by conferring a degree of degradability to the microgel platform, in that hydrolytically degradable microgels saw a decrease in IL-4 secretion and corresponding reduction in CD206+ macrophage presence compared to non-degradable microgels. Even minimal incorporation of the labile ester crosslinker, which does not lead to full degradation in the time window tested (i.e 0.25 mM EGBMA), provided differences in cellular and cytokine profiles, suggesting that the degradation profile of the material greatly influence the tissue response.

Although not investigated in this study, a range of parameters such as geometry, size, surface texture, stiffness and charge of materials can influence the host-implant interaction and the subsequent immune recognition and development of a FBR[18,43–45]. For example, FBR to spherical agarose microgels is modulated by the geometry and size of the implant, with larger sphere implants activating a lower FBR compared to smaller implants[43]. Likewise, chemical modification of PEG hydrogels with hydrophilic materials can modulate the FBR by reducing protein absorption and cellular attachment[44]. Important material properties such as stiffness are increasingly recognized to have a profound impact on driving cellular behaviors[45,46]. Stiffness-driven inflammatory responses to PEG hydrogels have been previously reported and thought to be associated to an increased immune cellular adhesion to stiffer surfaces[45]. This response has been recently attributed to the mechanosensitive transient receptor potential vanilloid 4 (TRPV4) independently of other biochemical cues[47]. The microgel implants used in this work swell significantly during hydrolysis-mediated degradation, and thus it cannot be ruled out that this dynamic shift in size post-implantation, together with decreasing stiffness leads to the modulation of cell infiltration observed in this study. It would be of interest to decouple these two parameters in the nondegradable implants to evaluate the singular effect of size of DTT crosslinked microgels on the FBR.

In sum, this study presents a cost-effective approach to conferring microgels with degradable features from PEG-4MAL macromers segmented via droplet microfluidics. Microgels with ester labile crosslinking junctions readily degrade *in vitro* and *in vivo*. Furthermore, the degradation profile impacts the immune response to the implant, with reduced type 1 associated cytokines and cells present when degradable microgels are delivered. The simplicity of this strategy and the efficiency of hydrolytic degradation of the resulting microgel population makes this approach attractive for regenerative medicine and drug delivery applications.

4. Experimental Section

Microfluidic Device Fabrication:

PDMS microfluidic devices were prepared as previously reported[21]. In brief, PDMS was cast using soft lithography and SU8 masters with microfluidic device patterns and heated to 110 °C for 20 minutes. The resulting PDMS microfluidic devices were removed from the wafer and bonded to glass slides and heated overnight to 70 °C.

PEG-4MAL Microgel Fabrication:

Polymer droplets were formed using a flow focusing microfluidic device with a 200 μm nozzle. The aqueous phase consisted of a 5% w/v PEG-4Mal (20 KDa, Laysan Bio) which had been previously reacted with a thiol-PEG-FITC (1 kDa, Nanocs). A co-flowing shielding phase consisted of mineral oil (Sigma) with 2% SPAN80 (Sigma). The crosslinker phase contained an emulsion of mineral oil/SPAN80 with DTT (Thermo) at a concentration of 15 mM. To render the microgels degradable various amounts of EGBMA (Sigma) were added to this crosslinker phase at 0.25, 0.5 and 1.0 mM concentrations. After fabrication, microgels were extracted from the oil phase by centrifugation, and washed with a 2% bovine serum albumin (Sigma)/PBS (corning) solution.

Microgel Sizing and Swelling:

Characterization of crosslinking phase on microgel size was measured after fabrication using a Biotek Cytation spectrophotometer. A sample of 50 μL in triplicates was placed in a glass bottom 6-well plate. Quantitative fluorescent intensity for each microgel was recorded for all samples. Droplet diameter was measured using the cellular analysis plug-in in the Cytation Gen software. For swelling studies, 1000 microgels were placed in 1 mL of PBS and placed in the incubator. Samples of 50 μL were taken every day and measured as described above. For FITC tracking studies, 1000 microgels were placed in 1 mL of PBS and solution was replaced every day. Collected supernatant fluorescence was measured using a Cytation 3 plate reader.

Microcapillary Mechanical Testing:

Microgel elastic properties were determined using pressure-driven capillary micromechanics[22]. At various time points (day 0, 3, 7), a microgel was inserted into the end of a tapered glass micropipette (Fivephoton Biochemicals) precoated with 1% (w/v) BSA in PBS (Figure S1). A high precision pressure regulator (Elveflow) was attached to the end of the micropipette, and pressure applied at various intervals (0, 2.5, 5, 7.5, 10, 15, 20, 25, 30, 40, 50, 60 kPa). When the microgel reached equilibrium (no longer moving in micropipette when external applied pressure balanced with internal elastic stress), an image was acquired on a microscope (10X; EVOS), and parameters were measured using ImageJ.

Viability assessments:

RAW 264.7 cells were co-cultured with 10,000 microgels for 7 days. Cell metabolic activity was measured via AlamarBlue (Invitrogen). The assay was performed at different time points (1, 2, 4 and 7 days). After 4 h of incubation, 100 μL of the supernatant was transferred to the wells of a 96-well plate and the OD was measured using a Cytation 3 imaging reader (Biotek) at 570 nm and 600 nm wavelengths.

Bone Marrow Derived Macrophage Co-culture:

Bone marrow was isolated from the femurs and tibias of 6-week-old male C57BL/6J mice. Bones were cleaned of soft tissue, one side was cut to expose the marrow, and they were inverted in a 200 μL pipet tip cut to fit in a 1.5 mL Eppendorf tube. The bones were then centrifuged at 10,000xg for 15 sec to pellet the marrow in the bottom of the Eppendorf tube.

Bones were discarded and cells were then resuspended in RBC Lysis Buffer (Biolegend 420302) to remove red blood cells. Cells were then washed in MACS buffer (DPBS pH 7.2, 0.5% BSA, 2mM EDTA) and monocytes were isolated using the Monocyte Isolation Kit (BM), mouse (Miltenyi Biotec 130–100-629) and LS columns (Miltenyi Biotec 130–042-401).

Monocytes were cultured in RPMI 1640 media (Gibco 11875–085) supplemented with 10% heat-inactivated fetal bovine serum, 1% pen/strep, and 20ng/mL murine M-CSF (Biolegend 574804) for 6 days in low-adherent plates. Cells were harvested and seeded with microparticles at a 1:10 ratio (10,000 cells/1000 microgels per well). M2 control macrophages were cultured in media supplemented with both 20 ng/mL murine M-CSF and 20 ng/mL murine IL-4 (Biolegend 574304). After 48 and 96 hr of co-culture cells were harvested and stained using the following markers: live dead (Zombie Violet, BioLegend 423113), CD45 (PE-Texas Red, BioLegend 103146), CD11b (PercpCy5.5, BioLegend 101228), F4/80 (FITC, BioLegend 123108), and CD206 (PECy7, BioLegend 141720). Samples were analyzed on a FACS-AriaIIIu flow cytometer (BD Biosciences).

Transplantation of microgels into mice:

All animal procedures were performed under protocols approved by Georgia Institute of Technology IACUC and in accordance with National Institutes of Health guidelines (IACUC approved protocol number A100326). Microgels were injected under the epidermis of 8–12-week-old BALB/cJ mice. The 100 μL injections consisted of about 3000 nondegradable or degradable hydrogels. All four conditions were injected into the same animal at independent sites to reduce any variability due to inherent biological differences across animals.

Microgel In Vivo Tracking:

Macromer was functionalized with a 1 KDa PEG labelled with AlexaFluor750 NHS ester (Thermo Fisher). Immediately after fabrication, 3000 microgels were injected under the epidermis in 100 μL of saline. Signal intensity and distribution were monitored longitudinally using an IVIS SpectrumCT imaging system (Perkin-Elmer). Data was analyzed using Living Image software. Regions of interest (ROIs) were drawn in defined pocket areas and quantified using Radiant Efficiency [p/s/sr]/[μW/cm2]. The ROIs were kept the same size for each group pocket at all time points and were appropriately sized to contain the fluorescent signal for each region, to ensure that the imaging data between individual donors can be compared across time. Intensity measurements were normalized to day 0 values.

MultiParametric Flow Analysis of Tissue Responses:

Tissue samples were obtained by a 12 mm biopsy punch and digested for 60 min at 37°C with an Accumax solution (Sigma). The digested tissue was passed through a 40 μm strainer and then washed twice with 1X PBS. Cells were washed stained for live/dead (Zombie violet, BioLegend 423113) and surface-stained with myeloid markers: CD45 (PE-Texas Red, BioLegend 103146), CD11b (PercpCy5.5, BioLegend 101228), F4/80 (FITC, BioLegend 123108), CD11c (BV785, BioLegend 117335), MHCII (APC-Cy7, BioLegend 107652), CD86 (APC, BioLegend 105012), CD206 (PECy7, BioLegend 141720). As well

as lymphoid markers: CD45 (BV711, BioLegend), CD3 (BV510, BioLegend 100233), CD4 (APC, BioLegend 100412), CD8 (PercpCy5.5, BioLegend 100732), CD25 (PECy7, BioLegend 102016), PD-1 (PE Texas Red, BioLegend 135227). Flow cytometry was performed with an BD Aria and analyzed in FCS express.

Cytokine Analysis:

Microgels were injected subcutaneously under the epidermis as described above. At set time points, a 12 mm biopsy punch in the surrounding injection site was used to remove the tissue. Samples were subsequently placed in RIPA buffer containing a protease inhibitor (Thermo). Samples were sonicated and centrifuged at 10,000 × g for 10 min at 4 °C to remove debris. Supernatant was frozen in liquid nitrogen and stored at −80 °C until analysis. Samples were analyzed using the Milliplex MAP Mouse Cytokine/Chemokine 32-plex assay (Millipore, MCYTMAG) on a Magpix multiplexing machine (Luminex) according to the manufacturer's instructions. PCA was conducted on all samples using the "prcomp" function in R and visualized using the "factoextra" package. Cytokine correlations were investigated using CytoMod[28,29]. For correlation analysis, values below the lower limit of detection were set to the lower limit of detection. Multi-variate linear regression with Log_{10} concentrations were modeled as a function of time. The "emmeans" package in R was used to assess pairwise differences in estimated marginal means between conditions, and Tukey's method was used to adjust for multiple comparisons.

Immunohistochemistry:

After euthanasia at day 30, a 12 mm biopsy punch in the surrounding injection site was used to remove the tissue, which was then fixed in 10% formalin solution overnight. Samples were subsequently processed with dehydration in graded ethanol solutions, cleared in xylene and paraffin-embedded. Sections were cut at 10 μm and slides were stained using hematoxylin and eosin (H&E), and IHC for macrophage pan marker CD68 (abcam, ab125212), and a nuclear staining (DAPI, Invitrogen D1306).

Statistical Analysis:

All experiments were performed on biological replicates. Sample size for each experimental group and statistical test used, with post hoc test where appropriate, to determine significant differences among groups are reported in the appropriate figure legend. Exact p values or meaning of significance symbol are presented in the legend. Data was analyzed with Graphpad Prism v9 (GraphPad Inc.). For cytokine analysis, concentration data was log transformed for normalization; analysis was performed in R, using the hclust, glm and lmmeans package. Experiments were not blinded, and no randomization was used.

Supplementary Material

Refer to Web version on PubMed Central for supplementary material.

Acknowledgements

We thank the core facilities at the Parker H. Petit Institute for Bioengineering and Bioscience at the Georgia Institute of Technology for the use and assistance with their shared equipment, services, and expertise. Funding:

This work was funded by the National Institutes of Health (U01 AI132817, R01 AR062920, and R01 AR062368 to A.J.G.), a JDRF Postdoctoral Fellowship (3-PDF-2019-743-A-N to M.M.C.), and National Science Foundation Graduate Fellowships (to M.D.H. and K.E.M.). Author contributions: M.M.C. synthesized and characterized microgels, performed tracking, transplants, and the collection of all data for manuscript. R.M.S. performed swelling and tracking experiments. K.E.M. helped with microgel injections, flow cytometry staining and analysis. M.D.H. performed all microcapillary mechanic testing. M.M.C., and A.J.G. conceived and designed all experiments. M.M.C., K.E.M., R.M.S. and A.J.G. wrote the manuscript.

References

(1). Daly AC; Riley L; Segura T; Burdick JA Hydrogel Microparticles for Biomedical Applications. Nat Rev Mater 2020, 5 (1), 20–43. 10.1038/s41578-019-0148-6. [PubMed: 34123409]

(2). Riley L; Schirmer L; Segura T Granular Hydrogels: Emergent Properties of Jammed Hydrogel Microparticles and Their Applications in Tissue Repair and Regeneration. Curr Opin Biotechnol 2019, 60, 1–8. 10.1016/j.copbio.2018.11.001. [PubMed: 30481603]

(3). Koh J; Griffin DR; Archang MM; Feng A-C; Horn T; Margolis M; Zalazar D; Segura T; Scumpia PO; Di Carlo D Enhanced In Vivo Delivery of Stem Cells Using Microporous Annealed Particle Scaffolds. Small 2019, 15 (39), 1903147. 10.1002/smll.201903147.

(4). Griffin DR; Weaver WM; Scumpia PO; Di Carlo D; Segura T Accelerated Wound Healing by Injectable Microporous Gel Scaffolds Assembled from Annealed Building Blocks. Nature Mater 2015, 14 (7), 737–744. 10.1038/nmat4294. [PubMed: 26030305]

(5). Muir VG; Qazi TH; Shan J; Groll J; Burdick JA Influence of Microgel Fabrication Technique on Granular Hydrogel Properties. ACS Biomater. Sci. Eng 2021, 7 (9), 4269–4281. 10.1021/acsbiomaterials.0c01612. [PubMed: 33591726]

(6). Foster GA; Headen DM; González-García C; Salmerón-Sánchez M; Shirwan H; García AJ Protease-Degradable Microgels for Protein Delivery for Vascularization. Biomaterials 2017, 113, 170–175. 10.1016/j.biomaterials.2016.10.044. [PubMed: 27816000]

(7). Photodegradable Hydrogels for Dynamic Tuning of Physical and Chemical Properties 10.1126/science.1169494 (accessed 2021 −10 −25).

(8). Carleton MM; Sefton MV Injectable and Degradable Methacrylic Acid Hydrogel Alters Macrophage Response in Skeletal Muscle. Biomaterials 2019, 223, 119477. 10.1016/j.biomaterials.2019.119477. [PubMed: 31521886]

(9). Jo YS; Gantz J; Hubbell JA; Lutolf MP Tailoring Hydrogel Degradation and Drug Release via Neighboring Amino Acid Controlled Ester Hydrolysis. Soft Matter 2009, 5 (2), 440–446. 10.1039/B814584A.

(10). Zustiak SP; Leach JB Hydrolytically Degradable Poly(Ethylene Glycol) Hydrogel Scaffolds with Tunable Degradation and Mechanical Properties. Biomacromolecules 2010, 11 (5), 1348–1357. 10.1021/bm100137q. [PubMed: 20355705]

(11). Rydholm AE; Anseth KS; Bowman CN Effects of Neighboring Sulfides and PH on Ester Hydrolysis in Thiol-Acrylate Photopolymers. Acta Biomater 2007, 3 (4), 449–455. 10.1016/j.actbio.2006.12.001. [PubMed: 17276150]

(12). PubMed Central Link

(13). Hunckler MD; Medina JD; Coronel MM; Weaver JD; Stabler CL; García AJ Linkage Groups within Thiol–Ene Photoclickable PEG Hydrogels Control In Vivo Stability. Advanced Healthcare Materials 2019, 8 (14), 1900371. 10.1002/adhm.201900371.

(14). Developing a pro-regenerative biomaterial scaffold microenvironment requires T helper 2 cells 10.1126/science.aad9272 (accessed 2022 −02 −11). 10.1126/science.aad9272.

(15). Sussman EM; Halpin MC; Muster J; Moon RT; Ratner BD Porous Implants Modulate Healing and Induce Shifts in Local Macrophage Polarization in the Foreign Body Reaction. Ann Biomed Eng 2014, 42 (7), 1508–1516. 10.1007/s10439-013-0933-0. [PubMed: 24248559]

(16). Host response to tissue engineered devices - ScienceDirect https://www.sciencedirect.com/science/article/pii/S0169409X98000234 (accessed 2021 −10 −25).

(17). Chung L; Maestas DR; Lebid A; Mageau A; Rosson GD; Wu X; Wolf MT; Tam AJ; Vanderzee I; Wang X; Andorko JI; Zhang H; Narain R; Sadtler K; Fan H; Čiháková D; Le Saux CJ; Housseau F; Pardoll DM; Elisseeff JH Interleukin 17 and Senescent Cells Regulate the Foreign Body

Response to Synthetic Material Implants in Mice and Humans. Sci Transl Med 2020, 12 (539), eaax3799. 10.1126/scitranslmed.aax3799. [PubMed: 32295900]

(18). Doloff JC; Veiseh O; de Mezerville R; Sforza M; Perry TA; Haupt J; Jamiel M; Chambers C; Nash A; Aghlara-Fotovat S; Stelzel JL; Bauer SJ; Neshat SY; Hancock J; Romero NA; Hidalgo YE; Leiva IM; Munhoz AM; Bayat A; Kinney BM; Hodges HC; Miranda RN; Clemens MW; Langer R The Surface Topography of Silicone Breast Implants Mediates the Foreign Body Response in Mice, Rabbits and Humans. Nat Biomed Eng 2021, 5 (10), 1115–1130. 10.1038/s41551-021-00739-4. [PubMed: 34155355]

(19). Sommerfeld SD; Cherry C; Schwab RM; Chung L; Maestas DR; Laffont P; Stein JE; Tam A; Ganguly S; Housseau F; Taube JM; Pardoll DM; Cahan P; Elisseeff JH Interleukin-36γ–Producing Macrophages Drive IL-17–Mediated Fibrosis. Science Immunology 2019, 4 (40), eaax4783. 10.1126/sciimmunol.aax4783. [PubMed: 31604843]

(20). Witherel CE; Sao K; Brisson BK; Han B; Volk SW; Petrie RJ; Han L; Spiller KL Regulation of Extracellular Matrix Assembly and Structure by Hybrid M1/M2 Macrophages. Biomaterials 2021, 269, 120667. 10.1016/j.biomaterials.2021.120667. [PubMed: 33450585]

(21). Headen DM; Aubry G; Lu H; García AJ Microfluidic-Based Generation of Size-Controlled, Biofunctionalized Synthetic Polymer Microgels for Cell Encapsulation. Advanced Materials 2014, 26 (19), 3003–3008. 10.1002/adma.201304880. [PubMed: 24615922]

(22). Wyss HM; Franke T; Mele E; Weitz DA Capillary Micromechanics: Measuring the Elasticity of Microscopic Soft Objects. Soft Matter 2010, 6 (18), 4550–4555. 10.1039/C003344H.

(23). Coronel MM; Martin KE; Hunckler MD; Barber G; O'Neill EB; Medina JD; Opri E; McClain CA; Batra L; Weaver JD; Lim HS; Qiu P; Botchwey EA; Yolcu ES; Shirwan H; García AJ Immunotherapy via PD-L1–Presenting Biomaterials Leads to Long-Term Islet Graft Survival. Science Advances 2020. 10.1126/sciadv.aba5573.

(24). Headen DM; Woodward KB; Coronel MM; Shrestha P; Weaver JD; Zhao H; Tan M; Hunckler MD; Bowen WS; Johnson CT; Shea L; Yolcu ES; García AJ; Shirwan H Local Immunomodulation with Fas Ligand-Engineered Biomaterials Achieves Allogeneic Islet Graft Acceptance. Nature Materials 2018, 17 (8), 732–739. 10.1038/s41563-018-0099-0. [PubMed: 29867165]

(25). Moore MW; Cruz AR; LaVake CJ; Marzo AL; Eggers CH; Salazar JC; Radolf JD Phagocytosis of Borrelia Burgdorferi and Treponema Pallidum Potentiates Innate Immune Activation and Induces Gamma Interferon Production. Infection and Immunity 2007, 75 (4), 2046–2062. 10.1128/IAI.01666-06. [PubMed: 17220323]

(26). Lynn AD; Bryant SJ Phenotypic Changes in Bone Marrow Derived Murine Macrophages Cultured on PEG-Based Hydrogels and Activated by Lipopolysaccharide. Acta Biomater 2011, 7 (1), 123–132. 10.1016/j.actbio.2010.07.033. [PubMed: 20674808]

(27). Curtis A; Calabro K; Galarneau J-R; Bigio IJ; Krucker T Temporal Variations of Skin Pigmentation in C57Bl/6 Mice Affect Optical Bioluminescence Quantitation. Mol Imaging Biol 2011, 13 (6), 1114–1123. 10.1007/s11307-010-0440-8. [PubMed: 20960234]

(28). Cohen L; Fiore-Gartland A; Randolph AG; Panoskaltsis-Mortari A; Wong S-S; Ralston J; Wood T; Seeds R; Huang QS; Webby RJ; Thomas PG; Hertz T A Modular Cytokine Analysis Method Reveals Novel Associations With Clinical Phenotypes and Identifies Sets of Co-Signaling Cytokines Across Influenza Natural Infection Cohorts and Healthy Controls. Frontiers in Immunology 2019, 10, 1338. 10.3389/fimmu.2019.01338. [PubMed: 31275311]

(29). Distinct inflammatory profiles distinguish COVID-19 from influenza with limited contributions from cytokine storm 10.1126/sciadv.abe3024 (accessed 2021 −10 −25).

(30). Schoenmakers RG; van de Wetering P; Elbert DL; Hubbell JA The Effect of the Linker on the Hydrolysis Rate of Drug-Linked Ester Bonds. Journal of Controlled Release 2004, 95 (2), 291–300. 10.1016/j.jconrel.2003.12.009. [PubMed: 14980777]

(31). Champion JA; Mitragotri S Role of Target Geometry in Phagocytosis. PNAS 2006, 103 (13), 4930–4934. 10.1073/pnas.0600997103. [PubMed: 16549762]

(32). Patel NR; Bole M; Chen C; Hardin CC; Kho AT; Mih J; Deng L; Butler J; Tschumperlin D; Fredberg JJ; Krishnan R; Koziel H Cell Elasticity Determines Macrophage Function. PLOS ONE 2012, 7 (9), e41024. 10.1371/journal.pone.0041024. [PubMed: 23028423]

(33). Féréol S; Fodil R; Labat B; Galiacy S; Laurent VM; Louis B; Isabey D; Planus E Sensitivity of Alveolar Macrophages to Substrate Mechanical and Adhesive Properties. Cell Motility 2006, 63 (6), 321–340. 10.1002/cm.20130.

(34). Thiols Decrease Human Interleukin (IL) 4 Production and IL-4-Induced Immunoglobulin Synthesis. J Exp Med 1995, 182 (6), 1785–1792. [PubMed: 7500023]

(35). Li Z; Bratlie KM How Cross-Linking Mechanisms of Methacrylated Gellan Gum Hydrogels Alter Macrophage Phenotype. ACS Appl. Bio Mater 2019, 2 (1), 217–225. 10.1021/acsabm.8b00562.

(36). Amer LD; Bryant SJ The in Vitro and in Vivo Response to MMP-Sensitive Poly(Ethylene Glycol) Hydrogels. Ann Biomed Eng 2016, 44 (6), 1959–1969. 10.1007/s10439-016-1608-4. [PubMed: 27080375]

(37). Lynn AD; Kyriakides TR; Bryant SJ Characterization of the in Vitro Macrophage Response and in Vivo Host Response to Poly(Ethylene Glycol)-Based Hydrogels. Journal of Biomedical Materials Research Part A 2010, 93A (3), 941–953. 10.1002/jbm.a.32595.

(38). Browning MB; Cereceres SN; Luong PT; Cosgriff-Hernandez EM Determination of the in Vivo Degradation Mechanism of PEGDA Hydrogels. J Biomed Mater Res A 2014, 102 (12), 4244–4251. 10.1002/jbm.a.35096. [PubMed: 24464985]

(39). Chan T; Pek EA; Huth K; Ashkar AA CD4+ T-Cells Are Important in Regulating Macrophage Polarization in C57BL/6 Wild-Type Mice. Cellular Immunology 2011, 266 (2), 180–186. 10.1016/j.cellimm.2010.10.002. [PubMed: 21040907]

(40). Tuzlak S; Dejean AS; Iannacone M; Quintana FJ; Waisman A; Ginhoux F; Korn T; Becher B Repositioning TH Cell Polarization from Single Cytokines to Complex Help. Nat Immunol 2021, 22 (10), 1210–1217. 10.1038/s41590-021-01009-w. [PubMed: 34545250]

(41). Kak G; Raza M; Tiwari BK Interferon-Gamma (IFN-γ): Exploring Its Implications in Infectious Diseases. Biomolecular Concepts 2018, 9 (1), 64–79. 10.1515/bmc-2018-0007. [PubMed: 29856726]

(42). O'Brien EM; Spiller KL Pro-Inflammatory Polarization Primes Macrophages to Transition into a Distinct M2-like Phenotype in Response to IL-4. Journal of Leukocyte Biology n/a (n/a) 10.1002/JLB.3A0520-338R.

(43). Veiseh O; Doloff JC; Ma M; Vegas AJ; Tam HH; Bader AR; Li J; Langan E; Wyckoff J; Loo WS; Jhunjhunwala S; Chiu A; Siebert S; Tang K; Hollister-Lock J; Aresta-Dasilva S; Bochenek M; Mendoza-Elias J; Wang Y; Qi M; Lavin DM; Chen M; Dholakia N; Thakrar R; Lacík I; Weir GC; Oberholzer J; Greiner DL; Langer R; Anderson DG Size- and Shape-Dependent Foreign Body Immune Response to Materials Implanted in Rodents and Non-Human Primates. Nature Mater 2015, 14 (6), 643–651. 10.1038/nmat4290. [PubMed: 25985456]

(44). Jansen LE; Amer LD; Chen EY-T; Nguyen TV; Saleh LS; Emrick T; Liu WF; Bryant SJ; Peyton SR Zwitterionic PEG-PC Hydrogels Modulate the Foreign Body Response in a Modulus-Dependent Manner. Biomacromolecules 2018, 19 (7), 2880–2888. 10.1021/acs.biomac.8b00444. [PubMed: 29698603]

(45). Blakney AK; Swartzlander MD; Bryant SJ The Effects of Substrate Stiffness on the in Vitro Activation of Macrophages and in Vivo Host Response to Poly(Ethylene Glycol)-Based Hydrogels. J Biomed Mater Res A 2012, 100 (6), 1375–1386. 10.1002/jbm.a.34104. [PubMed: 22407522]

(46). Irwin EF; Saha K; Rosenbluth M; Gamble LJ; Castner DG; Healy KE Modulus-Dependent Macrophage Adhesion and Behavior. Journal of Biomaterials Science, Polymer Edition 2008, 19 (10), 1363–1382. 10.1163/156856208786052407. [PubMed: 18854128]

(47). Goswami R; Arya RK; Sharma S; Dutta B; Stamov DR; Zhu X; Rahaman SO Mechanosensing by TRPV4 Mediates Stiffness-Induced Foreign Body Response and Giant Cell Formation. Science Signaling 14 (707), eabd4077. 10.1126/scisignal.abd4077.

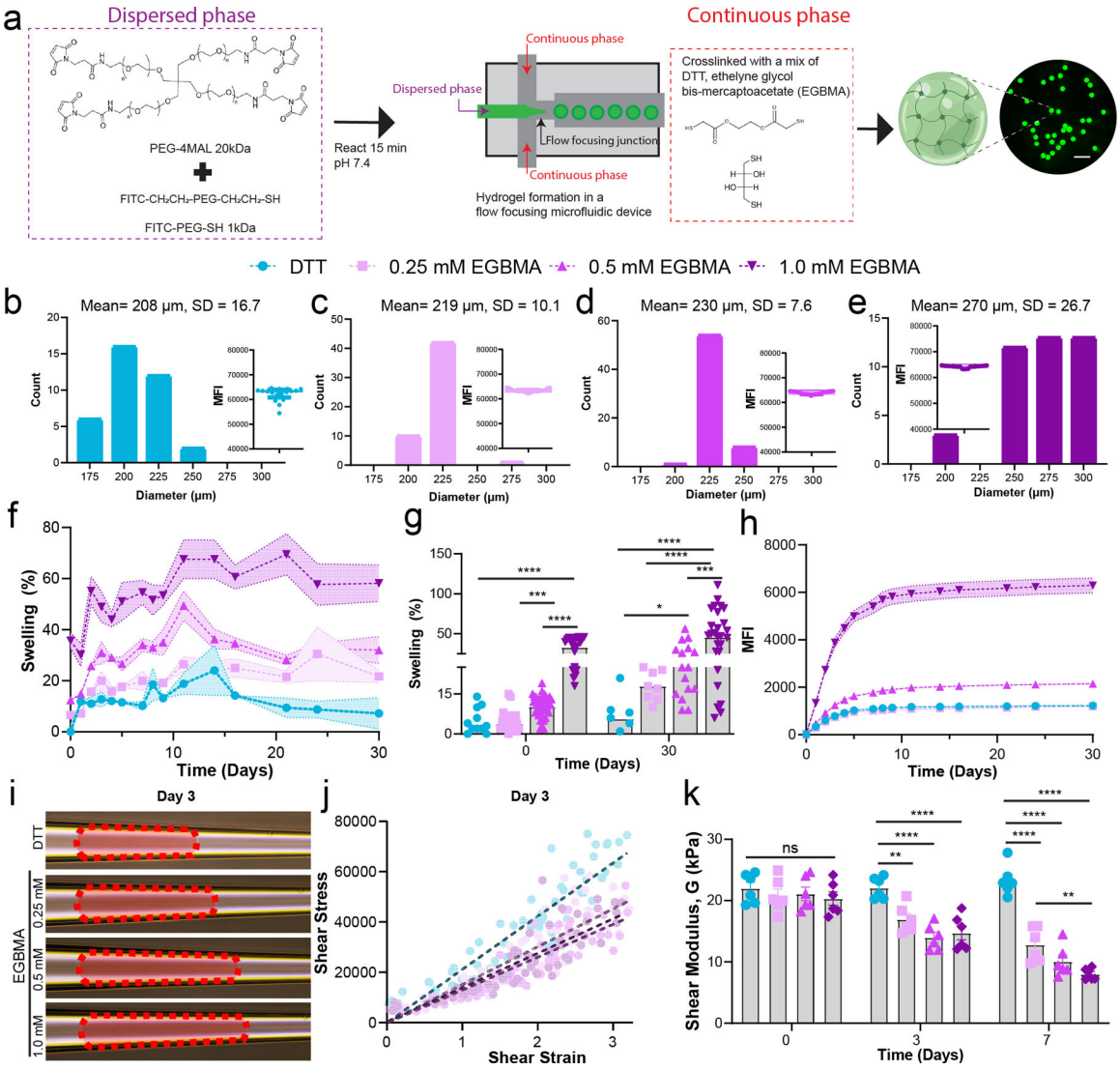

Figure 1.

Hydrolytically degradable microgels can be fabricated by the addition of ester-containing dithiol crosslinkers. a) PEG-4MAL macromer is modified with linear PEG FITC and segmented through a flow-focusing microfluidic chip with a continuous phase containing small dithiol molecules, DTT and EGBMA. This results in monodisperse microgels that can be fluorescently tracked. Scale bar 1 mm. b–e) Size distribution of microgels based on EGBMA concentration in the oil phase. Inset represents the intensity of individual microgels post-fabrication, demonstrating similar modification of the macromer backbone with the linear PEG-FITC tracker, minimum n = 36, pooled from 3 independent microfludic runs. f,g) Microgel swelling in an aqueous buffer is directly proportional to the molar concentration of EGBMA linker in the crosslinking phase, minimum n = 6 per sample. h) Tracking of released PEG-FITC in solution is dependent on EGBMA concentration in microgels. i) Day 3 images of microgels deformed by an applied pressure in a tapered microcapillary. j) Shear stress versus strain for confined microgels fabricated with varying concentrations of EGBMA after 3 days of incubation in an aqueous buffer, n = 6, >60 points total. k)

Quantification of shear modulus of all microgel formulations after different time exposures to aqueous buffer, n = 6. All data presented as average ± s.e.m. unless otherwise stated, swelling data analyzed using a mixed-effect model, with Tukey correction for multiple comparisons; Shear modulus was analyzed with a two-way ANOVA with Tukey corrections for multiple comparisons. * $p < 0.05$, ** $p < 0.01$, *** $p < 0.005$, **** $p < 0.0001$.

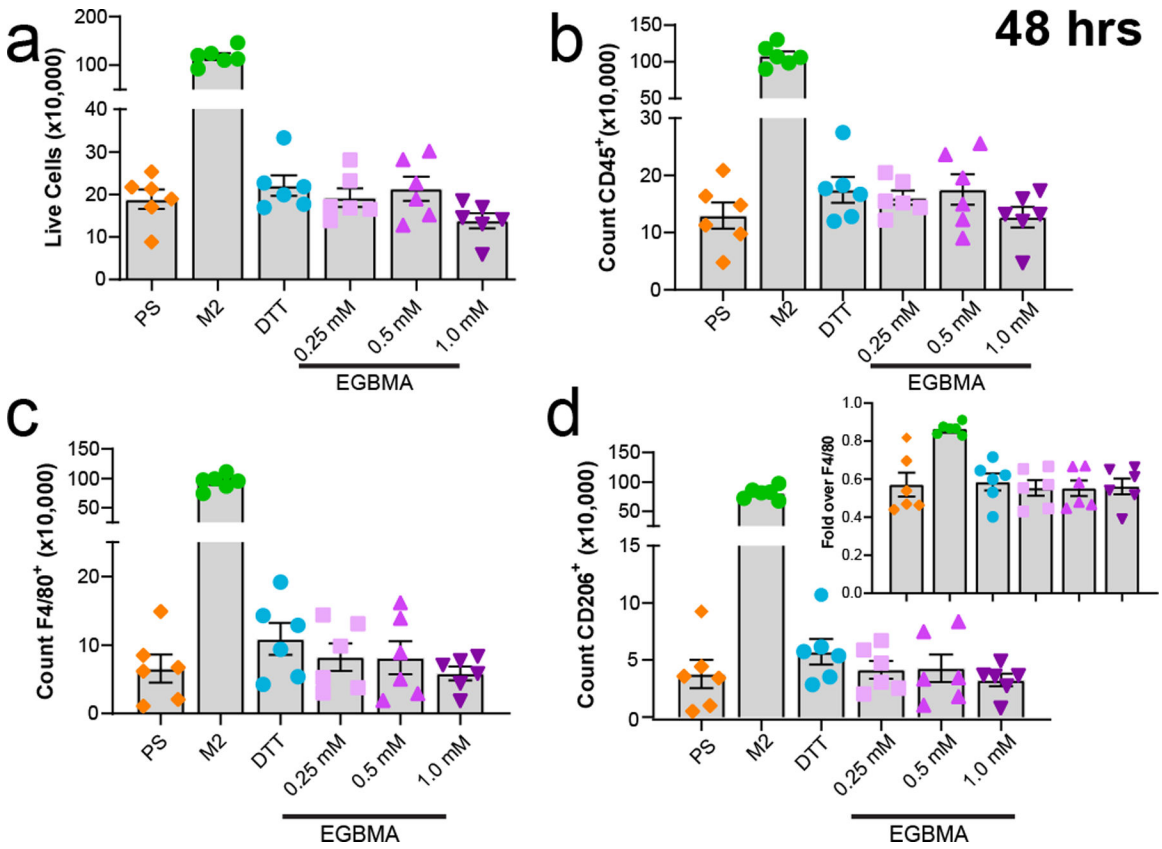

Figure 2.

Microgel co-culture with monocytes does not induce activation in the absence of adhesion cues and inflammatory signals. a–d) Cell survival at 48 h post-incubation does not reveal any changes due to microparticle presence in co-culture. Expression of markers CD45, F4/80, CD206 is equivalent across all groups tested. d-inset represents fold expression of CD206 over all cells expression F4/80 in co-culture. n = 6 per group, all data presented as average ± s.e.m. Data was analyzed with one-way ANOVA with Tukey corrections for multiple comparisons.

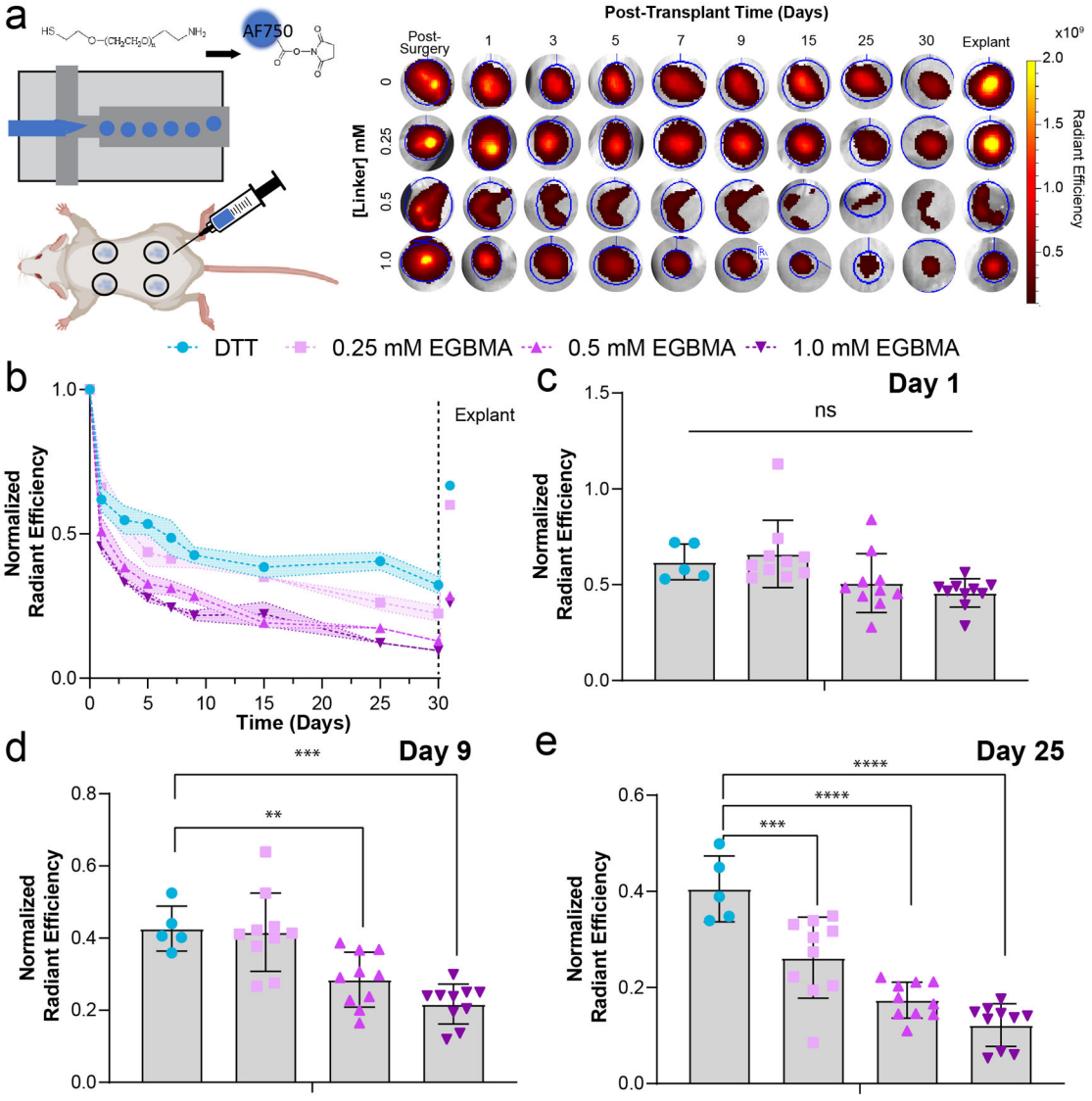

Figure 3.

Degradation of subcutaneous microgel implants is directly proportional to the concentration of the EGBMA linker. a) Scheme of microgel fabrication with a near-infrared PEG linker and injection in a dorsal subcutaneous pocket. Representative images of implant pockets at different timepoints post-injection and after explant. b) Average normalized radiant efficiency for all formulations throughout the course of a month and after explant (points following vertical dashed line). c–e) quantification of normalized radiant efficiency at days 0, 9, and 25 post-implantation. All data presented as average ± s.d. minimum of n = 5 recipients for DTT, n = 10 for all other groups. P values calculated using one-way ANOVA with Dunnett multiple comparison analysis, **p < 0.05, ***p < 0.0005, ****p < 0.0001.

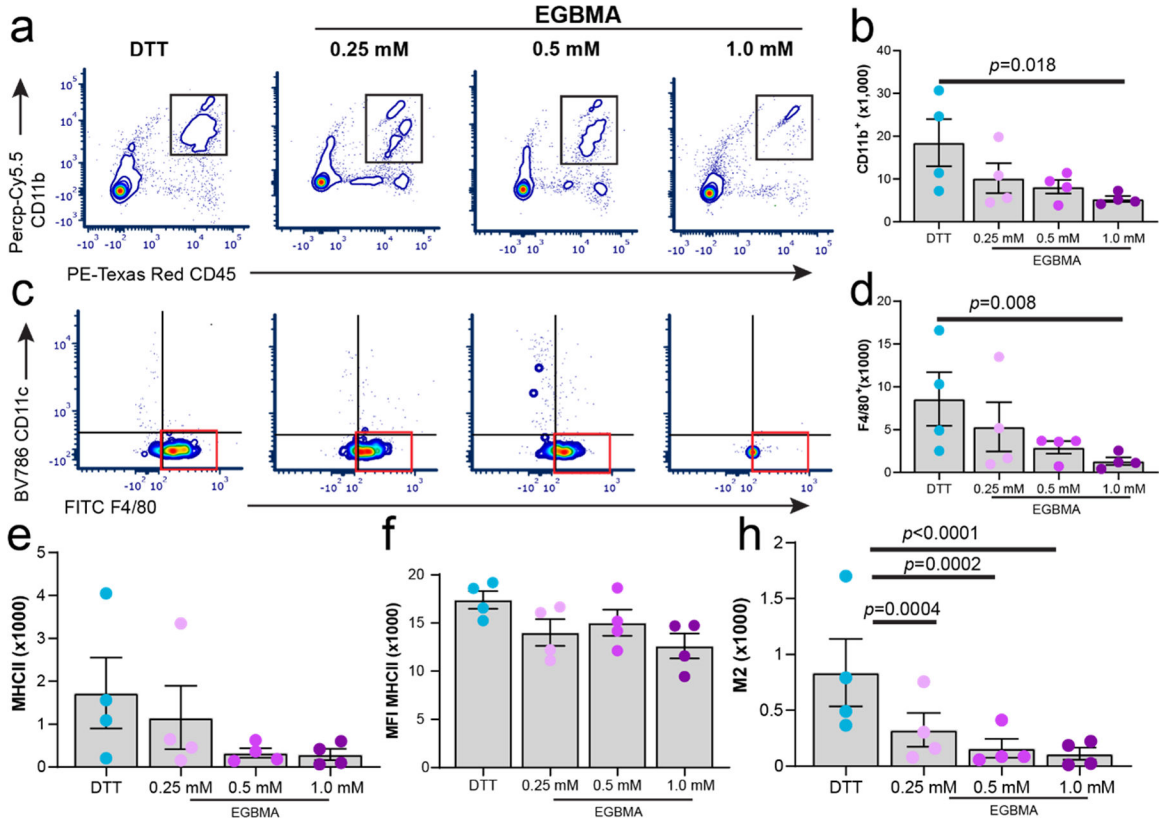

Figure 4.

Myeloid cell recruitment and polarization are modulated by the degradation of the synthetic microgel implant at 7 days post-injection. a–h) flow cytometry analysis and quantification of myeloid markers CD11b, F4/80, MHCII, and CD206 from subcutaneous implant pockets containing different formulations of nondegradable and degradable microgels. All data presented as average ± s.e.m. Sample size, n = 4. P values were calculated using one-way ANOVA, correcting for multiple comparisons by controlling the false discovery rate.

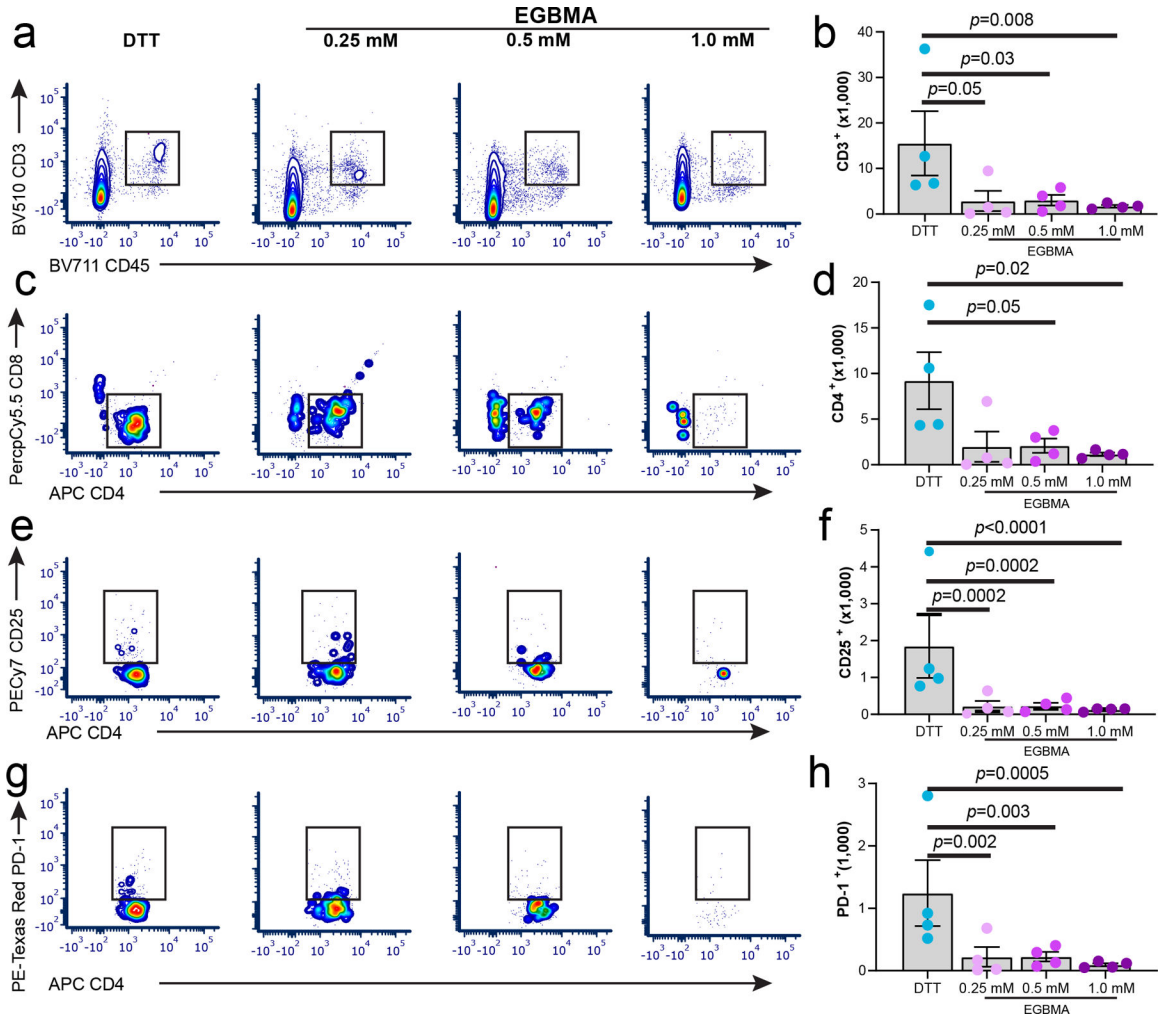

Figure 5.

Lymphocyte cell recruitment is controlled by the degradation of the synthetic microgel implant 7 days post-injection. a–h) Flow cytometry analysis and quantification of lymphocyte markers CD3, CD4, CD8, CD25, and PD-1 from subcutaneous implant pockets containing different formulations of nondegradable and degradable microgels. All data presented as average ± s.e.m. Sample size n = 4. P values were calculated using one-way ANOVA, correcting for multiple comparisons by controlling the false discovery rate.

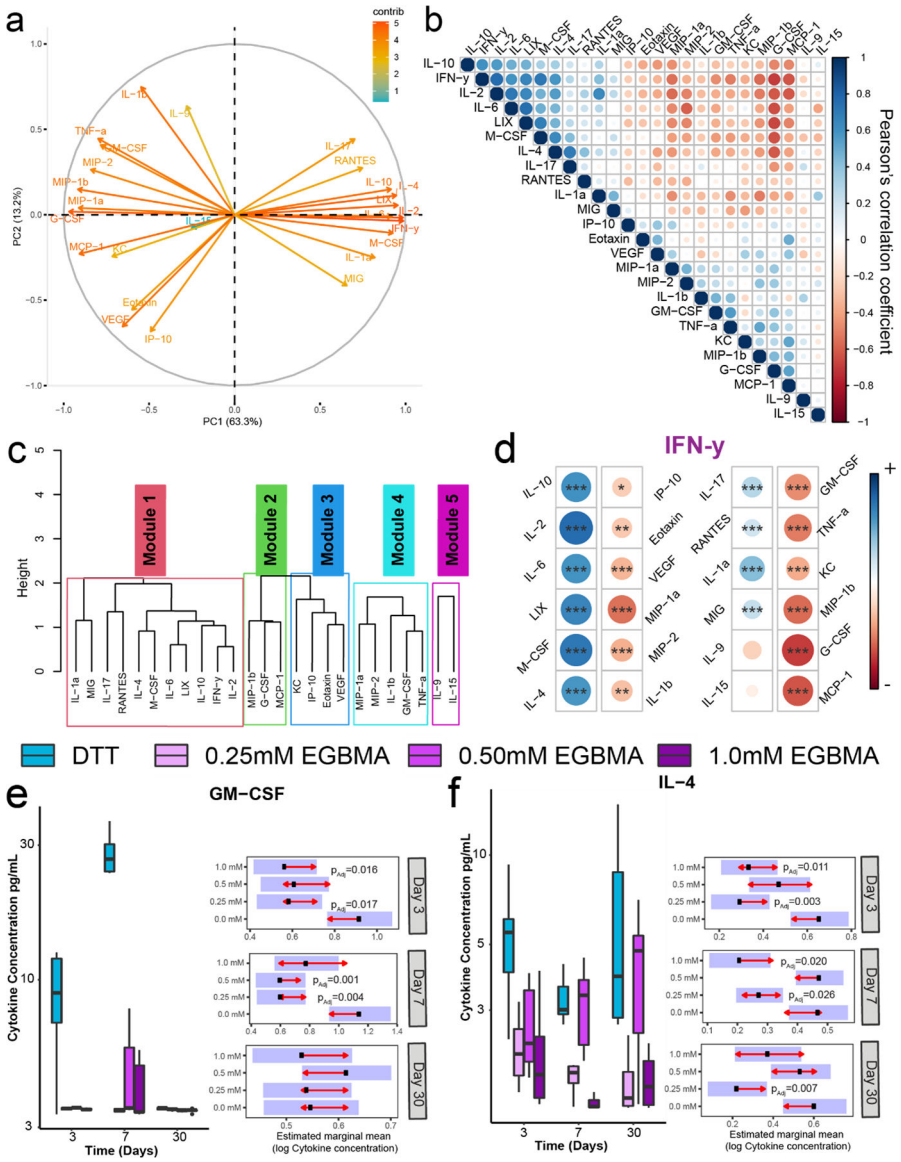

Figure 6.

Cytokine responses to implantable synthetic microgels are dynamic and dominated by IFN-γ responses which can be altered by the degradation potential of the implantable material. a) Principal component analysis of 32 cytokines measured in implant tissues from animals receiving different synthetic microgel formulations. Arrows color and directions indicate the contribution to each dimension of the PCA. b) Cytokine correlations for all cytokines measured are assessed using Pearson's correlation coefficient. c) Left: hierarchical clustering of cytokines based on Pearson's correlation, dendrogram, and cytokine name denotes module membership. d) Correlation plots for all cytokines against IFN-γ. e,f) Box plots show cytokine concentrations for GM-CSF and IL-4 with raw values plotted on the log10 scale. Samples size n = 6. Presented P values are from estimated marginal means (EMM) comparisons.